Supporting Information

Molecular Control of the Nanoscale: Effect of Phosphine Chalcogenide Reactivity on CdS-CdSe Nanocrystal Composition and Morphology

T. Purnima A. Ruberu,[1,2] Haley R. Albright,[1] Brandon Callis,[2,3] Brittney Ward,[2,3] Joana Cisneros,[2,3] Hua-Jun Fan,[2,3] Javier Vela[1,2]*

[1]Department of Chemistry, Iowa State University, Ames, IA 50011, [2]US DOE Ames Laboratory, Ames, IA 50011, [3]Department of Chemistry, Prairie View A&M University, Prairie View, TX 77446

Computational details

Calculations were carried out using the Gaussian 03 package[1] running on CenterOS based Linux cluster at the Department of Chemistry, Prairie View A&M University. The Tao-Perdew-Staroverov-Scuseria (TPSS) method,[2] implemented in Gaussian 03, was used for all geometry optimization, solvation modeling and frequency calculations. A new generation of density functional, TPSS matches or exceeds in accuracy most prior functionals, including the popular B3LYP-with-hybrid-exchange functional.[3] TPSS can recognize relatively weak interactions (such as agostic interactions) while B3LYP significantly underestimates them.[4] Because hydrogen atoms in the modeling system do not play significant roles in our study, a 6-311G* basis set[5,6] was used for all elements in the modeling system. Not applying polarization functions on H's far away from phosphorous does not significantly degrade computational precision and accuracy and can considerably accelerate the calculations.[7] All structures were fully optimized and frequency analyses were performed until minima were achieved, with zero imaginary vibrational frequencies as derived from vibrational frequency analysis. Thermodynamic functions including enthalpies, entropies and free energies, were calculated at 298.15 K and 1 atm. To examine basis set effect, a Dunning/Huzinaga full double zeta[8] with Stuttgart/Dresden effective core potentials basis set (SDD) and a triple-zeta Dunning's correlation consistent basis set (cc-pVTZ)[9] were used for all atoms with TPSS functionals to perform a single point energy (SPE) calculation. The Polarizable Continuum Model (PCM) using the integral equation formalism variant (IEFPCM) was applied to compute aqueous solvation free energies for all compounds and reactions.

To better understand these phenomena, we first turned our attention to computational modeling of the factors behind precursor reactivity at the atomic level. We focused our attention on chalcogenide (sulfide and selenide) derivatives, $R_3P=E$, of five commercially available phosphines, R_3P: Hexamethyl-phosphorous-triamide (HMPT), trioctyl-phosphine (TOP), tributylphosphine (TBP), diphenylpropyl-phosphine (DPP), and triphenylphosphite (TPP). We consider phosphine-chalcogen to be the most reactive bond, thus we focus on the geometric and electronic properties around the phosphorous center. Selected optimized geometry parameters are listed in Table S1, and relative energetic parameters with zero-point energy correction ($\Delta E°_{ZPE}$), enthalpy ($\Delta H°$) and free energies ($\Delta G°$) corrected to room temperature for the reaction $R_3P + S \rightarrow R_3P=E$ (E = S, Se) are shown in Table S2. P-R# represent bond lengths between P the connecting atom of ligand R. For example, P-R1 represents P-O1 bond length in TPP, and P-N1 bond length in HPT. R2 and R3 group are phenyl groups in DPP.

Table S1. Selected bond lengths (Å) and angles (deg.) for optimized geometries of TPP, DPP, TBP, TOP, HPT, and their chalcogenide (sulfide and selenide) derivatives.

	TPP	TPPS	DPP	DPPS	TBP	TBPS	TOP	TOPS	HPT	HPTS
Sulfides										
P-S		1.921		1.974		1.978		1.978		1.982
P-R1	1.676	1.631	1.878	1.854	1.880	1.855	1.880	1.855	1.804	1.748
P-R2	1.675	1.630	1.855	1.844	1.880	1.854	1.880	1.855	1.804	1.748
P-R3	1.671	1.630	1.861	1.847	1.881	1.854	1.880	1.855	1.804	1.748
R1-P-R2	95.8	99.5	99.1	106	99.1	104.3	99.3	104.2	101.4	104.6
R1-P-R3	96.6	99.3	103.1	105.2	99.1	104.5	98.8	104.6	101.4	104.6
R2-P-R3	96.2	99.1	101.2	103.3	99.1	104.3	99.1	104.4	101.4	104.6
S-P-R1		118.2		113.6		114.1		114.2		114.0
S-P-R2		118.3		114.0		114.2		114.2		114.0
S-P-R3		118.4		113.7		114.3		114.2		114.0
Selenides										
	TPP	TPPSe	DPP	DPPSe	TBP	TBPSe	TOP	TOPSe	HPT	HPTSe
P-Se		2.073		2.129		2.131		2.131		2.141
P-R1	1.676	1.633	1.878	1.857	1.880	1.857	1.880	1.858	1.804	1.749
P-R2	1.675	1.633	1.855	1.849	1.880	1.858	1.880	1.857	1.804	1.749
P-R3	1.671	1.632	1.861	1.846	1.881	1.857	1.880	1.857	1.804	1.749
R1-P-R2	95.8	98.9	99.1	103.4	99.1	104.1	99.3	104.2	101.4	104.8
R1-P-R3	96.6	99.0	103.1	105.3	99.1	104.1	98.8	104.1	101.4	104.8
R2-P-R3	96.2	99.4	101.2	105.3	99.1	104.4	99.1	104.4	101.4	104.8
Se-P-R1		118.6		113.5		114.3		114.2		113.9
Se-P-R2		118.5		113.9		114.3		114.3		113.9
Se-P-R3		118.3		113.9		114.3		114.3		113.9

In the optimized geometries, P=S bond lengths slightly increase from TPPS (1.921 Å), to DPP (1.974 Å), TBPS (1.978 Å), TOPS (1.978 Å), and HPTS (1.982 Å). Similarly, P=Se bond lengths slightly increase from TPPSe (2.073 Å), to DPPSe (2.129 Å), TBPSe (2.131 Å), TOPSe (2.131 Å), and HPTSe (2.141 A). However, this is not an indication of relative P=E (S, Se) bond strength, but rather a consequence of the size and steric bulk of the substituents on phosphorous. All R-P-R bond angles increase when binding with S or Se. For S, the smallest change is with TPP and HPT, ~3 deg from 96 to 99 deg and from 101 to 104 deg, respectively. Also for S, the biggest change is with DPP, where one C(alkyl)-P-C(phenyl) bond angle changes almost 7 deg from 99.1 to 106.0 deg. Interestingly, the other two bond angles of DPP only changes ~2 deg from 103.1 to 105.2 and from

101.2 to 103.3 deg. TBP and TOP has relatively big bond angle change of 5-6 deg. All P-R bond lengths decrease upon binding S or Se. P-R bond lengths in TPP and HPT decrease by 3%, while in DPP, TBP and TOP they only decrease by 1%.

Table S2. The relative reaction energetic parameters with zero-point energy correction ($\Delta E°_{ZPE}$), enthalpy ($\Delta H°$) and free energies ($\Delta G°$) corrected to room temperature.

	$\Delta E°$	$\Delta E°_{ZPE}$	$\Delta H°$	$\Delta G°$	$\Delta E°$	$\Delta E°_{Solv}$	$\Delta E°_{Solv}$
Basis set	6-311G*				cc-pVTZ	6-311G*	SDD
Sulfides							
TPP + S → TPPS	-76.20	-74.06	-74.87	-64.66	-79.55	-67.12	-69.04
DPP + S → DPPS	-75.21	-73.35	-74.01	-63.91	-80.03	-78.18	-90.00
TBP + S → TBPS	-79.88	-77.71	-78.41	-68.38	-83.42	-84.13	-94.49
TOP + S → TOPS	-82.86	-80.99	-81.57	-71.60	-86.95	-87.33	-97.83
HPT + S → HPTS	-89.77	-86.71	-87.57	-77.60	-91.78	-90.80	-96.48
Selenides							
TPP + Se → TPPSe	-62.42	-60.84	-61.40	-51.67	-63.77	-61.27	-56.31
DPP + Se → DPPSe	-62.96	-61.63	-62.07	-52.10	-65.98	-65.17	-77.17
TBP + Se → TBPSe	-67.04	-65.43	-65.87	-56.23	-69.75	-70.95	-82.99
TOP + Se → TOPSe	-70.07	-68.60	-68.99	-59.10	-72.98	-74.16	-86.28
HPT + Se → HPTSe	-76.81	-74.38	-75.00	-65.22	-77.52	-77.21	-83.68

As shown in Table S2, chalcogenide (sulfide or selenide) formation is exothermic or "downhill" (the chalcogenide product is always thermodynamically more stable than the reactants). According to Gibbs free energy changes, $\Delta G°$, phosphine-chalcogenide stability clearly decreases in the order: HPTS > TOPS > TBPS > DPPS ~ TPPS. Just for curiosity, we also used the Polarizable Continuum Model (PCM) with the integral equation formalism variant (IEFPCM) to compute hypothetical free energies of polar solvent solvation for these reactions. In the PCM model,[10,11] the solvent is represented by a dielectric continuum model. The solute molecule is then embedded into a cavity surrounded by a dielectric continuum of permittivity. The results are summarized under $\Delta E°_{Solv}$ heading in Table S2. These solvated values are not a good correlation for our studies, because our experiments were run at high temperature in non-polar hydrocarbon phosphine solvents. We also used two new basis sets calculate single point energies (SPE) using 6-311G* optimized geometries. The results are listed in the Table S2. The SPE $\Delta E°$ results with the cc-pVTZ basis set mirror those with the 6-311G* basis set. The SPE $\Delta E°_{solv}$ results with the SDD basis set also have the same trend as with the 6-311G* basis set. All basis sets put TPP and DPP as the most reactive species in the series. It is interesting to note that the $\Delta E°$ difference between the two extreme cases TPP and HPT in the sulfide reaction is ~13 kcal/mol, while the solvation energy difference

$\Delta E°_{Solv}$ between them is ~23 kcal/mol. In comparison, the Se reaction shows a $\Delta E°$ difference between TPP and HPT of ~14 kcal/mol vs. a $\Delta E°_{Solv}$ of ~16 kcal/mol.

As shown above, the geometric changes between S and Se precursors are subtle (Table S1, but their energetic parameters show big differences (Table S2). This prompted us to pay a closer look at the electronic structure and charge distribution of these molecules.[12] The commonly used Mülliken population analysis,[13,14] based on projecting the electron density onto a reference basis set, is strongly dependent on the basis set used.[15] On the other hand, atomic polar tensor (APT)[16] atomic populations, based on the tensor of the derivatives of dipole moment with respect to atomic Cartesian coordinates, exhibit modest basis set sensitivity and can model the atomic population more realistically.[17] APT results are readily available from the Gaussian output. APT charges can provide important insights into the charge distribution of the molecule and are better than natural orbital population analysis and electrostatic potential CHELPG methods.[18]

Table S3. Calculated Mülliken and APT charge distribution on P, S and Se atoms.

	Dipole	Mülliken Charges			APT charges		
	moment	P	Δ(PE-P)	E	P	Δ(PE-P)	S
TPP	1.781	0.841	-	-	1.948	-	-
DPP	1.335	0.493	-	-	0.568	-	-
TBP	1.263	0.500	-	-	0.421	-	-
TOP	1.314	0.414	-	-	0.430	-	-
HPT	0.801	0.759	-	-	0.988	-	-
TPPS	0.593	0.947	0.106	-0.326	2.570	0.622	-0.606
DPPS	4.954	0.688	0.195	-0.455	1.547	0.979	-0.701
TBPS	4.783	0.532	0.031	-0.335	1.267	0.846	-0.663
TOPS	4.656	0.538	0.125	-0.340	1.298	0.867	-0.673
HPTS	2.563	0.704	-0.055	-0.301	1.854	0.866	-0.726
TPPSe	0.441	1.011	0.170	-0.376	2.476	0.528	-0.510
DPPSe	4.894	0.743	0.249	-0.475	1.440	0.872	-0.599
TBPSe	4.785	0.649	0.148	-0.386	1.171	0.750	-0.584
TOPSe	4.656	0.655	0.241	-0.391	1.197	0.767	-0.593
HPTSe	2.670	0.840	0.081	-0.374	1.769	0.781	-0.663

Table S3 lists Mülliken and atomic polar tensor (APT) atomic charges on P, S and Se atoms for all phosphines and phosphine-chalcogenide precursors. Both Mülliken and APT charges place positive charge on P and negative charges on S and Se. However, when comparing the amount of charge change upon chalcogenide formation (under the "Δ(PE-P)" column in Table S3), Mülliken charges show no clear pattern. On the other hand, APT charge analysis shows a progressive increase of positive charge on the P atom upon chalcogenide formation.

Figure S1 shows the highest occupied molecular orbital (HOMO) of HPTS, HPTSe, TPPS, and TPPSe. The

HOMO's of these sulfides and selenides are based on the 1-node p-orbital interaction with sulfur or selenide. However, there is a big difference between HPT and TPP compounds. While all the HOMO orbitals are π-bond in character, TPPSe has smallest contribution from phenyl substituens, while HPTS and HPTSe have large contributions from nitrogen (amide) substituents. This is because the oxygen bridge between phenyl and P not only creates a distance gap for their electron densities to interact, but also because the oxygen lone pairs do not facilitate the π-interaction. In contrast, the nitrogen atom in the amine group is directly connected to P and the geometry of amine group is situated perfectly for the π-interaction with the P atom. This is clearly demonstrated by TPPS, where the 1-node π-interaction from the phenyl ring is clearly isolated from that of P=S π-bond. This is one of the keys to the predicted high reactivity of phosphite-chalcogenide precursors. With extensive π-interaction between P atom and its associated amides, HPTS and HPTSe bind S and Se more strongly. The weaker π-interaction in TPP is also observed in the APT population analysis. TPP shows the lowest APT charge change upon binding to chalcogen (0.622, S; 0.528, Se) compared with DPP (0.979, S; 0.872, Se), TBP (0.846, S; 0.750, Se), TOP (0.867, S; 0.767, Se), and HPT (0.866, S; 0.781, Se). Overall, this is consistent with our experiemental observations: TPPS and TPPSe are unstable and very reactive chalcogen sources. APT population analysis seems to suggest that higher charge polarization at P atom increases the reactivity of the precursor; the charge on P atom is the highest for TPP.

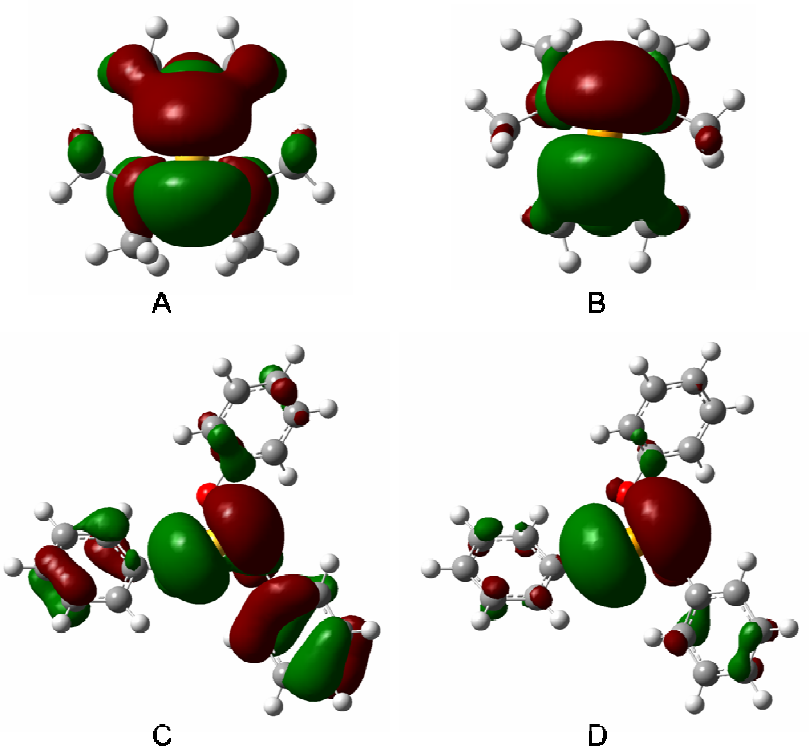

Figure S1. Highest occupied molecular orbital (HOMO) of HPTS (A), HPTSe (B), TPPS (C) and TPPSe (D).

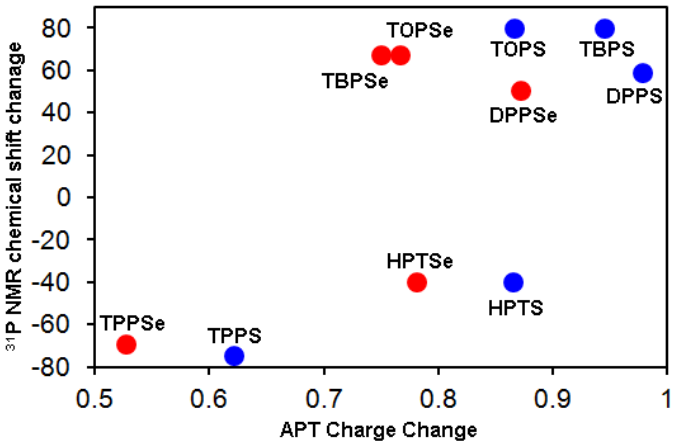

Figure S2. A plot of ^{31}P NMR chemical shift against calculated APT charge change upon phosphine-chalcogenide formation.

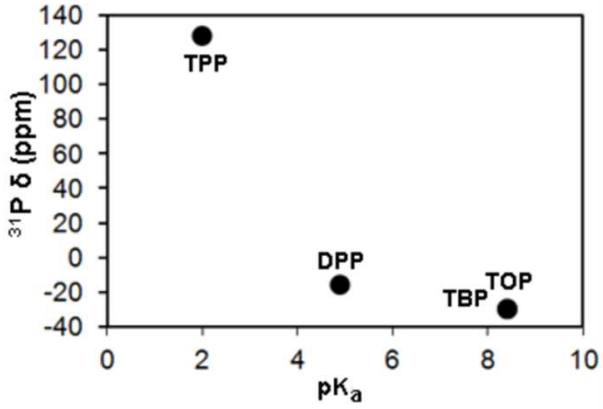

Figure S3. A plot of ^{31}P δ against phosphine pK$_a$ values.

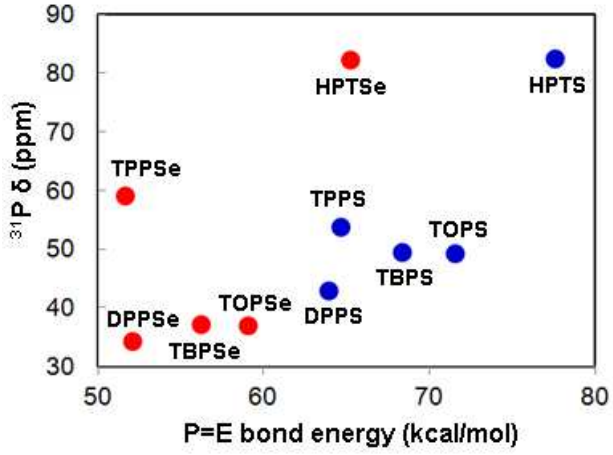

Figure S4. Experimentally measured ^{31}P NMR chemical shifts (δ/ppm) of phosphine-chalcogenide precursors as a function of calculated P=E (E = S, Se) bond strength (estimated as -ΔG° for phosphine-chalcogenide

formation, Table S1).

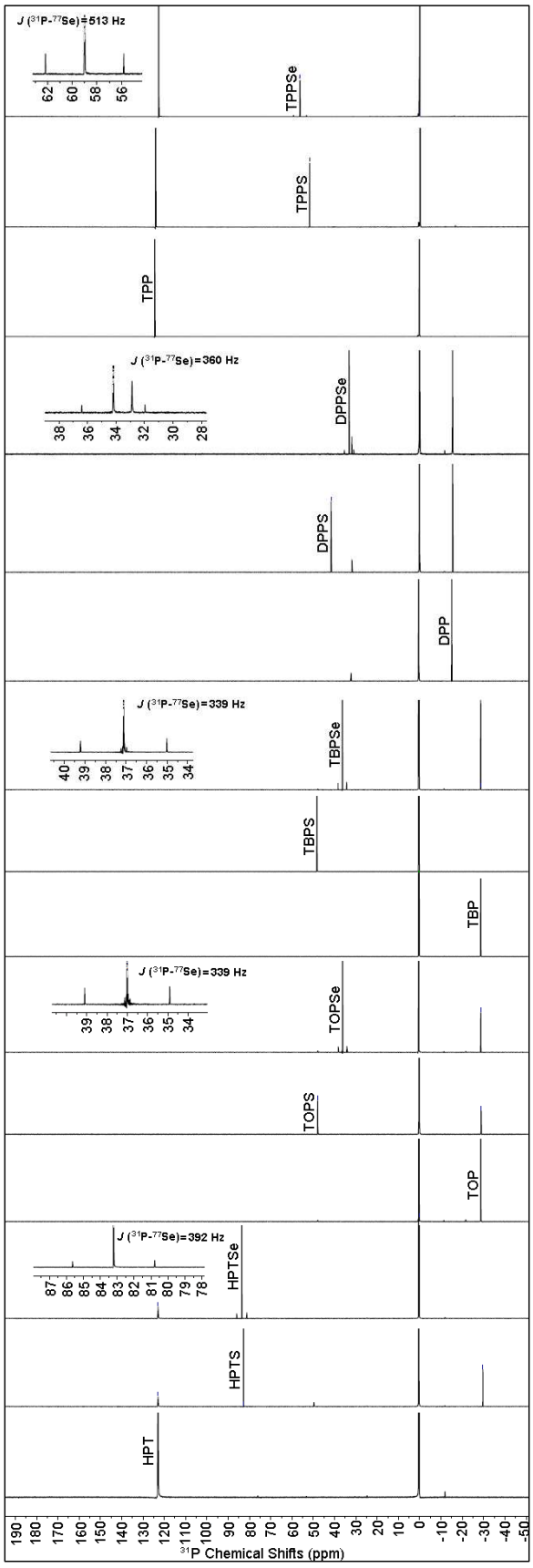

Figure S5. A stack plot of ^{31}P NMR spectra of different phosphines and phosphine-chalcogenides.

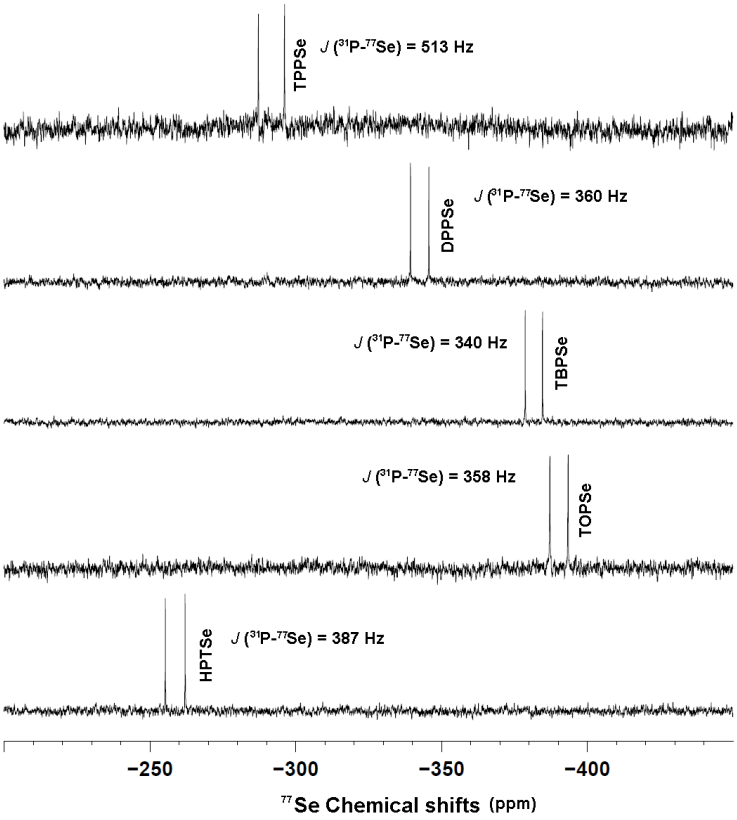

Figure S6. Stack plot of ^{77}Se NMR spectra of phosphine-selenides.

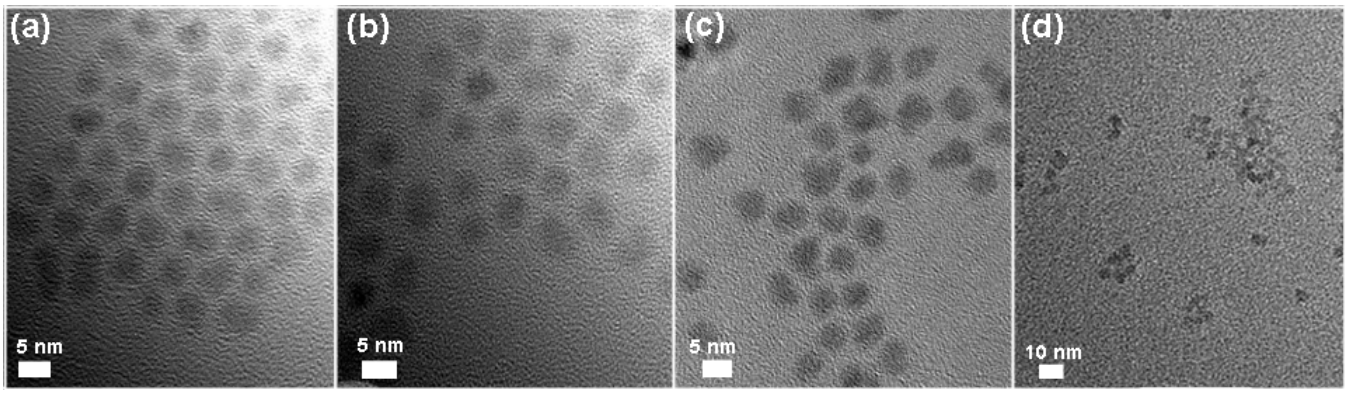

Figure S7. Sample TEM images of $CdS_{1-x}Se_x$ QDs synthesized with (a) DPPSe and TOPS (1:3) (b) TOPSe and DPPS (1:3) (c) TBPSe and DPPS (1:9) (d) HPTSe and TBPS (1:19).

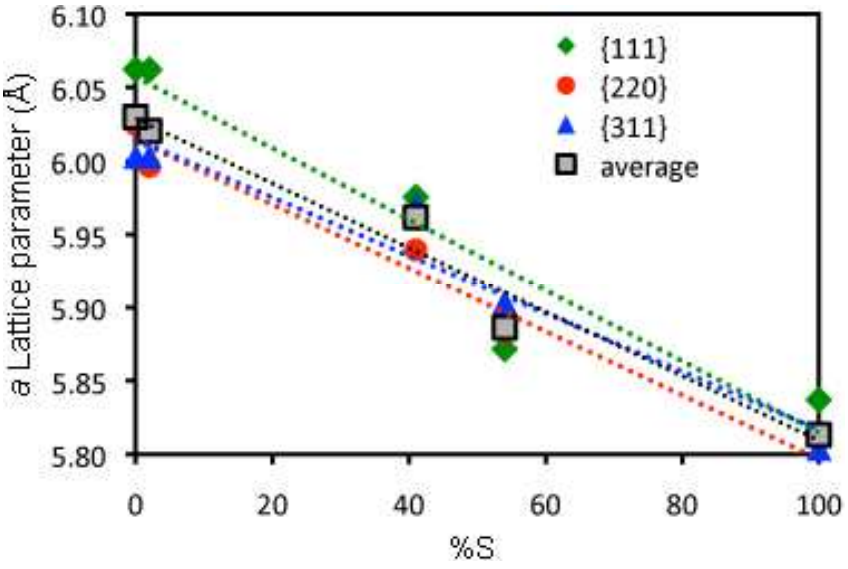

Figure S8. Alternative Vegard's plot for $CdS_{1-x}Se_x$ dots showing the variation in cubic *a* lattice parameter as a function of %S.

References

[1] Gaussian 03, Revision D.01. Frisch, M. J.; Trucks, G. W.; Schlegel, H. B.; Scuseria, G. E.; Robb, M. A.; Cheeseman, J. R.; Montgomery, J. A.; Vreven, T.; Kudin, K. N.; Burant, J. C.; Millam, J. M.; Iyengar, S. S.; Tomasi, J.; Barone, V.; Mennucci, B.; Cossi, M.; Scalmani, G.; Rega, N.; Petersson, G. A.; Nakatsuji, H.; Hada, M.; Ehara, M.; Toyota, K.; Fukuda, R.; Hasegawa, J.; Ishida, M.; Nakajima, T.; Honda, Y.; Kitao, O.; Nakai, H.; Klene, M.; Li, X.; Knox, J. E.; Hratchian, H. P.; Cross, J. B.; Bakken, V.; Adamo, C.; Jaramillo, J.; Gomperts, R.; Stratmann, R. E.; Yazyev, O.; Austin, A. J.; Cammi, R.; Pomelli, C.; Ochterski, J. W.; Ayala, P. Y.; Morokuma, K.; Voth, G. A.; Salvador, P.; Dannenberg, J. J.; Zakrzewski, V. G.; Dapprich, S.; Daniels, A. D.; Strain, M. C.; Farkas, O.; Malick, D. K.; Rabuck, A. D.; Raghavachari, K.; Foresman, J. B.; Ortiz, J. V.; Cui, Q.; Baboul, A. G.; Clifford, S.; Cioslowski, J.; Stefanov, B. B.; Liu, G.; Liashenko, A.; Piskorz, P.; Komaromi, I.; Martin, R. L.; Fox, D. J.; Keith, T.; Al-Laham, M. A.; Peng, C. Y.; Nanayakkara, A.; Challacombe, M.; Gill, P. M. W.; Johnson, B.; Chen, W.; Wong, M. W.; Gonzalez, C.; Pople, J. A. Gaussian, Inc., Wallingford CT, 2004.

[2] Tao, J. M.; Perdew, J. P.; Staroverov, V. N.; Scuseria, G. E. Climbing the Density Functional Ladder: Nonempirical Meta-Generalized Gradient Approximation Designed for Molecules and Solids. *Phys. Rev. Lett.* **2003**, *91*, 12129–12137.

[3] Staroverov, V. N.; Scuseria, G. E.; Tao, J. M.; Perdew, J. P. Comparative Assessment of a New Nonempirical Density Functional: Molecules and Hydrogen-Bonded Complexes. *J. Chem. Phys.* **2003**, *119*, 12129–12137.

[4] Fan, Y. B.; Bacon, S.; Kolade, A.; Wasiu, A.; Fan, H.-J. A DFT Study on the Mechanism of Wolff Rearrangement in a Five Member Iridacycle. *Intl. Conf. Comp. Sci.* **2010**, *1*, 2659–2667.

[5] Hehre, W. J.; Ditchfie, R.; Pople, J. A. Self-Consistent Molecular-Orbital Methods 12. Further Extensions of Gaussian-Type Basis Sets for Use in Molecular-Orbital Studies of Organic Molecules. *J. Chem. Phys.* **1972**, *56*, 2257–2261.

[6] Krishnan, R.; Binkley, J. S.; Seeger, R.; Pople, J. A. Self-Consistent Molecular-Orbital Methods 20. Basis Set for Correlated Wave Functions. *J. Chem. Phys.* **1980**, *72*, 650–654.

[7] Fan, Y. B.; Hall, M. B. The Competition Between Allene and Butadiene in the Carbon-Hydrogen Bond Activation Initiated by a Tungsten Allyl Complex: A DFT Study. *Organometallics* **2005**, *24*, 3827–3835.

[8] Dunning, T. H.; Hay, P. J. In *Modern Theoretical Chemistry*, vol. 3.; Schaefer, H. F., Ed.; Plenum: New York, 1976; pp. 1–28.

[9] Kendall, R. A.; Dunning, T. H.; Harrison, R. J. Electron Affinities of the First-Row Atoms Revisited. Systematic Basis Sets and Wave Functions. *J. Chem. Phys.* **1992**, *96*, 6796–806.

[10] Miertuš, S.; Scrocco, E.; Tomasi, J. Electrostatic Interaction of a Solute with a Continuum: A Direct Utilization of Ab Initio Molecular Potentials for the Prevision of Solvent Effects. *Chem. Phys.* **1981**, *55*, 117–29.

[11] Tomasi, J.; Mennucci, B.; Cammi, R. Quantum Mechanical Continuum Solvation Models. *Chem. Rev.* **2005**, *105*, 2999–3093.

[12] Bachrach, S. M. In *Reviews in Computational Chemistry*, vol. V; Lipkowitz, K. B. and Boyd, D. B., Eds.; VCH: New York, 1995.

[13] Mulliken, R. S. Electronic Structures of Polyatomic Molecules and Valence II. General Considerations. *Phys. Rev.* **1932**, *41*, 49–71.

[14] Mulliken, R. S. Electronic Population Analysis on LCAO-MO Molecular-Wave Functions I-IV. *J. Chem. Phys.* **1955**, *23*, 1833–1840; 1841–1846; 2338–2342; 2343–2346.

[15] De Proft, F.; Martin, J. M. L.; Geerlings, P. On the Performance of Density Functional Methods for Describing Atomic Populations, Dipole Moments and Infrared Intensities. *Chem. Phys. Lett.* **1996**, *250*, 393–401.

[16] Cioslowski, J. A New Population Analysis Based on Atomic Polar Tensors. *J. Am. Chem. Soc.* **1989**, *111*, 8333–8336.

[17] Amarasekara, A. S.; Lewis, D.; Nayani, S. L.; Timofeeva, T. V.; Fan, H.-J. X-Ray Crystallography and Computational Studies of the Structure of Bis-nitrone,2,5-bis{[methyl(oxido)imino]phenyl}furan. *J. Molec. Struc.* **2010**, *977*, 175–179.

[18] Breneman, C. M.; Wiberg, K. B. Determining Atom-Centered Monopoles from Molecular Electrostatic Potentials. The Need for High Sampling Density in Formamide Conformational Analysis. *J. Comput. Chem.* **1990**, *11*, 361–73.